Isothermal Thickening and Thinning Processes in Low Molecular Weight Poly(ethylene oxide) Fractions Crystallized from the Melt. 5. Effect of Chain Defects

Seung-Wook Lee, Erqiang Chen, Anqiu Zhang, Yeocheol Yoon, Bong Seok Moon, Sangkug Lee, Frank W. Harris, and Stephen Z. D. Cheng*

Maurice Morton Institute and Department of Polymer Science, The University of Akron, Akron, Ohio 44325-3909

Ernst D. von Meerwall

Department of Physics, The University of Akron, Akron, Ohio 44325

Benjamin S. Hsiao and Ravi Verma

Central Research and Development Department, Experimental Station, E. I. du Pont de Nemours and Company, Wilmington, Delaware 19880-0302

Jerome B. Lando

Department of Macromolecular Science, Case Western Reserve University, Cleveland, Ohio 44106-2699

Received January 12, 1996; Revised Manuscript Received October 1, 1996[⊗]

ABSTRACT: Two-arm poly(ethylene oxide) (PEO) fractions with different molecular weights (MWs) have been prepared. For each fraction, both arms have equal lengths of MW = 2300 or 5500. The MWs and molecular weight distributions of two-arm PEOs after fractionation are determined from vapor pressure osmometry, gel permeation chromatography, and light scattering. Compared to linear PEO fractions with similar molecular lengths, the two-arm PEOs can be viewed as linear chains with a well-defined defect at the center of the molecule. Self-diffusion coefficients of the two-arm PEOs are measured and compared with linear PEOs having molecular lengths equivalent to both a single arm and a whole molecule. The crystallization behavior of the PEOs is monitored *via* wide angle X-ray diffraction, small angle X-ray scattering, and differential scanning calorimetry. Over a wide undercooling range, the two-arm PEO molecules do not appear to recognize the defects at the center of the chains during the initial stage of crystallization. During this stage of crystallization, they form nonintegral folding chain crystals having a fold length longer than the arm length. The defects are recognized only after the initial crystallization and gradually migrate to the lamellar surface through an apparent thinning process. The crystallization kinetics of the two-arm PEOs are significantly slower than those of the linear PEO molecules having a length equivalent to a single arm as well as a combined length of two arms. The melting behavior of the two-arm PEOs is, however, similar to that of linear PEOs which have a length of a single arm. The single lamellar crystal morphology of the two-arm PEOs observed *via* polarized light microscopy shows the faceting−rounding−refaceting effect with decreasing undercooling. Nevertheless, refaceted single crystals at very low undercoolings have a rectangular shape rather than the hexagonal one generally observed in the linear PEOs. This difference in the single crystal morphology may be caused by a change in the folding directions due to the large defects on the lamellar surfaces.

Introduction

Over the past 6 years, our research has focused on the study of a well-defined model system, a series of low molecular weight (MW) poly(ethylene oxide) (PEO) fractions, to understand the mechanisms of polymer crystallization. This study was also motivated by the observation of nonintegral folding chain (NIF) crystals in pure *n*-alkanes reported in the middle 1980s.[1,2] Our investigation has involved several steps. The first step was to experimentally identify the existence of the NIF crystals in the PEO fractions *via* real-time synchrotron small angle X-ray scattering (SAXS). Over a wide undercooling range, NIF crystals formed prior to being transformed into integral folding chain (IF) crystals. Although the NIF crystal is thermodynamically less stable, kinetically it grows faster.[3−9] The study of the MW dependence of NIF crystal formation in these PEOs has indicated that, with increasing MW, the transformation of the NIF → IF crystals is increasingly hampered by a decrease in the thermodynamic driving force between the initial NIF and the final IF crystals and an increase in the molecular motion barrier. At sufficiently long chain lengths, the NIF crystals may be permanently retained. The lamellar thickness shows a linear relationship with reciprocal undercooling, as predicted by nucleation theory.[8] Since these low MW PEOs possess OH end groups, hydrogen bonding has been found in both the solid and the melt.[9] It has been speculated that the hydrogen bonding may play an important role in the IF crystal formation.[10−17] However, other end groups were also introduced into the low MW PEOs, and the IF crystals were, in many cases, observed.[18−25] We have systematically investigated the end group effect on the formation of NIF crystals and found that despite the type of end groups, NIF crystals exist in the PEO fractions. Furthermore, the NIF crystals exist for a longer period of time by increasing the end group size (from OCH_3 to $OC(CH_3)_3$ to OC_6H_5).[4,9]

* To whom correspondence should be addressed.

[⊗] Abstract published in *Advance ACS Abstracts,* December 15, 1996.

S0024-9297(96)00048-4 CCC: $12.00

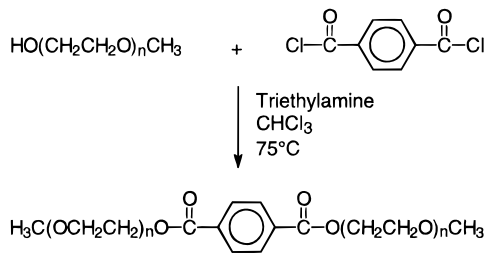

Figure 1. Chemical reaction scheme of the synthesis of two-arm PEO.

This suggests that a sliding motion of the chain molecules along the *c*-axis in the crystals may occur during and after crystallization.[26−28]

To extend our understanding of polymer crystallization, we have synthesized and isolated two-arm PEOs with both 2300 and 5500 MW arms. Therefore, the total MWs of these two fractions are 4600 and 11 000 (excluding the MW of the coupling agent, which is 164.1 g/mol), respectively. It is expected that, during the crystallization of these two-arm PEOs, the defect at the center of each chain should affect the crystal growth kinetics, which may lead to different phase transformation behavior and crystal morphology. Comparisons of the transition behavior and morphology with those of linear low MW PEOs having the molecular lengths equivalent to both a single arm and the whole chain have been carried out to understand the effect of chain defects.

Experimental Section

Materials Synthesis. Two low MW PEO fractions [α-methoxy-ω-hydroxypoly(ethylene oxide)] ($HO(CH_2CH_2O)_nCH_3$) with MW = 2300 and 5500 were purchased from Aldrich Chemical Co. These PEOs possess one hydroxyl and one methoxy end group. Further fractionation was carried out in our laboratory. The coupling agent 1,4-benzenedicarbonyl dichloride was also purchased from Aldrich.

The two-arm PEO fractions were prepared *via* a reaction of the PEO with 1,4-benzenedicarbonyl dichloride in chloroform. The linear PEO (MW = 2300 or 5500) fraction and a coupling agent were dried under vacuum and further freeze-dried in dry benzene. Twenty grams of PEO was dissolved in 200 mL of chloroform with triethylamine (8 mL) and maintained in an oil bath at 75 °C. During vigorous stirring, 1,4-benzenedicarbonyl dichloride was very slowly added in stoichiometric amounts and the reaction mixture was kept at 75 °C for 2 days under a nitrogen atmosphere. The product was then precipitated in dried ethyl ether and filtered. In order to eliminate insoluble impurities, the product was redissolved in dried benzene and filtered several times. After filtering, the polymer was reprecipitated and transferred to a vacuum oven and dried overnight. Figure 1 shows the chemical reaction scheme and schematic shape of the two-arm PEOs.

Since the reaction product contains a mixture of the unreacted linear "parent" PEO and the newly formed two-arm PEO, the product was fractionated by a nonsolvent addition method to obtain the pure two-arm PEO fraction. The PEO sample obtained after the reaction was dissolved in chloroform (1 wt %). Ethyl ether was gradually added as a nonsolvent while the solution was vigorously stirred until the solution became milky. After several hours, the precipitated PEOs were separated by filtration. The remaining solution was further fractionated using the same procedure. Each fraction was refractionated at least eight times until a pure two-arm PEO was obtained.

Molecular Characterization. Gel permeation chromatography (GPC) experiments in tetrahydrofuran (THF) at 30 °C were carried out to measure the number-average MW and polydispersities. GPC was also used to examine each fraction during the fractionation procedure. The effective MW range for the columns used was 500−600 000. The GPC was calibrated using standard linear PEO fractions in the same MW range. Fourier transform infrared spectroscopy (FTIR, Mattson Galaxy 5020) measurements were carried out in the range between 2500 and 4000 cm^{-1} to study the end groups of the PEOs. The films of linear and two-arm PEO fractions were solution cast on NaCl pellets for FTIR measurements. A Knauer vapor pressure osmometer was used to determine the number-average MW in toluene at 40 °C. For the calibration of the vapor pressure osmometer, sucrose octaacetate was used in the same solvent. The concentration of the sample solution (in g/kg) was kept similar to that of the calibration solution. Finally, light scattering (LS, Wyatt Dawn F) experiments were also conducted to insure the accuracy of the polydispersities by measuring the weight-average MWs.

Differential Scanning Calorimetry. Differential scanning calorimetry (DSC, DuPont 910) experiments were carried out to study the isothermal crystallization and melting behavior of the linear and two-arm PEO fractions. The DSC was calibrated with an indium standard. The sample weight was maintained at approximately 0.5 mg and the pan weights were kept constant within an accuracy of ±0.001 mg. Isothermal crystallization was conducted by quenching the samples from the isotropic melt to the preset crystallization temperature. In the low undercooling range a self-seeding technique was used for the isothermal crystallization as described previously.[13] After annealing at the self-seeding temperature T_s ($T_s = T_m - 1.5$ °C), for 20 min, the samples were shifted to the preset isothermal crystallization temperature. The crystallized samples were then heated to above the melting temperature (T_m) with a heating rate of 5 °C/min.

Nuclear Magnetic Resonance. The self-diffusion coefficients of the PEO fractions in the melt were determined by a pulsed-gradient spin-echo (PGSE) nuclear magnetic resonance (NMR) method.[29−31] The principle echo on-resonance without Fourier transform was measured using radio frequency phase-sensitive detection. Its attenuation in the presence of a pair of applied magnetic field gradient pulses was also detected. For all samples, measurements at three temperatures (65.5, 85.5, and 90.5 °C) were conducted. The PEO critical MW, M_c, at which entangled behavior is first observed in a monodisperse melt, was $M_c = 4400$ based on Ferry's compilation.[32]

Wide Angle X-ray Diffraction. Wide angle X-ray diffraction (WAXD) was used to determine the crystal structure and crystallinity of the linear and two-arm PEOs *via* a Rigaku 12-kW rotating anode generator in the reflection mode. The wavelength of the monochromated X-rays from Cu Kα radiation was 0.154 nm. Time-resolved isothermal synchrotron WAXD experiments were also carried out to monitor the structural development during the crystallization process. They were simultaneously conducted with time-resolved SAXS experiments at a synchrotron X-ray beam line (3B) of the National Synchrotron Light Source (NSLS) at Brookhaven National Laboratory (BNL). The beam wavelength was 0.155 nm.

Small Angle X-ray Scattering. Time-resolved synchrotron SAXS experiments were carried out at the synchrotron X-ray beam line 3B of the NSLS at BNL. Isothermal crystallization measurements were carried out on a customized two-chamber hot stage. Temperature control was ±0.3 °C.[6−9] A position sensitive proportional counter was used to record the diffraction patterns. The counter was calibrated with a duck tendon which shows scattering peaks at $2\theta = 0.1432°$ (61.6 nm), 0.2864° (30.8 nm), and 0.4340° (20.3 nm). The Lorentz correction was performed by multiplying the intensity, I (counts per second), by s^2 ($s = 2 \sin \theta/\lambda$, where λ is the wavelength of synchrotron X-ray radiation). The correlation function method was also applied to obtain the fold lengths of PEO lamellar crystals.[33]

Polarized Light Microscopy. Linear crystal growth rates were measured using a polarized light microscope (PLM) (Olympus HB-2) in conjunction with a Mettler FP-82HT hot stage. The hot stage temperature was calibrated with sharp melting point standards. The precision of the temperature control was ±0.1 °C. The samples were heated above the

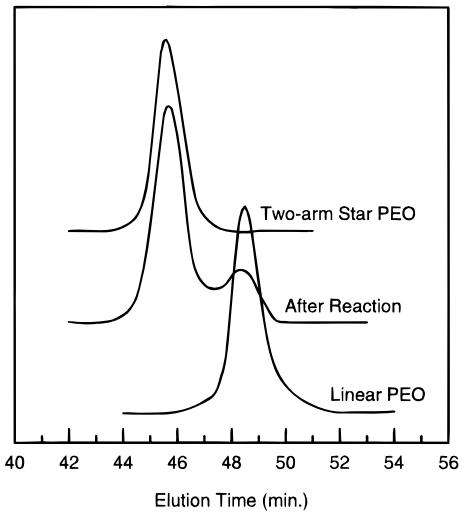

Figure 2. GPC diagrams of the linear "parent" PEO and unfractionated and fractionated two-arm PEOs.

Table 1. Molecular Characteristics of Linear and Two-Arm PEO Fractions

	M_n[a]	M_n[b]	M_w/M_n[c]	M_a[d]	average length (nm)[e]
linear PEO	2200	2300	1.04	–	14.5
	5500	5500	1.05	–	34.8
two-arm PEO	4500	4600	1.05	2300	29.7
	11000	11500	1.06	5500	70.3

[a] Number-average molecular weight from GPC. [b] Number-average molecular weight from VPO. [c] Polydispersities from GPC, and independently checked *via* LS by measuring the weight-average MWs. [d] Number-average molecular weight of each arm. [e] The average chain lengths were calculated from the equation $l = M_n/d$, $d = 152.8$[11] for the linear fractions. For the two-arm PEO fractions, the average chain lengths were calculated *via* doubling the linear fraction length and adding the size of the coupling agent.

equilibrium melting temperature for 2 min and quenched to a preset crystallization temperature. The crystal growth rates were measured (a standard deviation of ±7%) after the temperature reached equilibrium. The self-seeding technique[13] was also used in the low undercooling range for PLM growth rate measurements and single crystal observations. After growing single crystals, the samples were quickly immersed into a dry ice/acetone mixture to generate tiny spherulites of 1-5 μm in size on the edges of single lamellar crystals in order to achieve self-decoration for observation of the single crystal morphologies.[13]

Results and Discussion

Molecular and Structure Analysis. Figure 2 is the GPC diagram of the linear "parent" PEO and the unfractionated and fractionated two-arm PEOs. It is evident that the unfractionated two-arm PEO contained some of the linear "parent" PEO. After the fractionation, the diagram of the two-arm PEO shows that the MW distribution is unimodal and narrow. The number- and weight-average MWs obtained from GPC calibrated with standard linear PEO fractions are listed in Table 1. The number-average MWs of the PEO fractions determined by VPO are also included in Table 1. Weight-average MWs were obtained by light scattering as an additional check on the polydispersity.

FTIR has been used to examine the possible existence of hydrogen bonding of the end groups of the linear PEOs. The absorption band at 3500 cm^{-1} in Figure 3 originates from hydrogen bonding and OH stretching

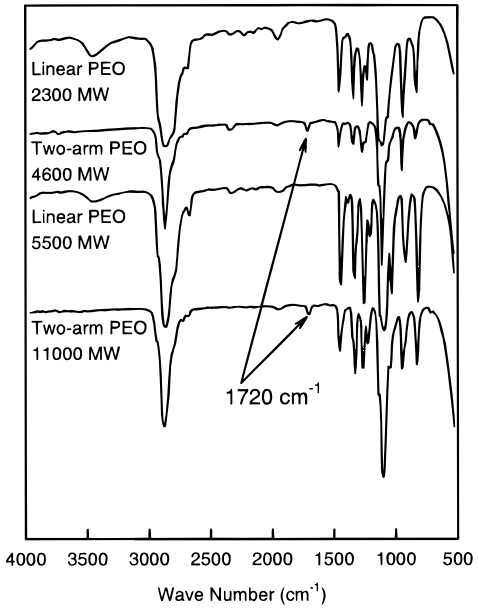

Figure 3. FTIR spectra of the linear and two-arm PEOs with arm molecular weights of 2300 and 5500.

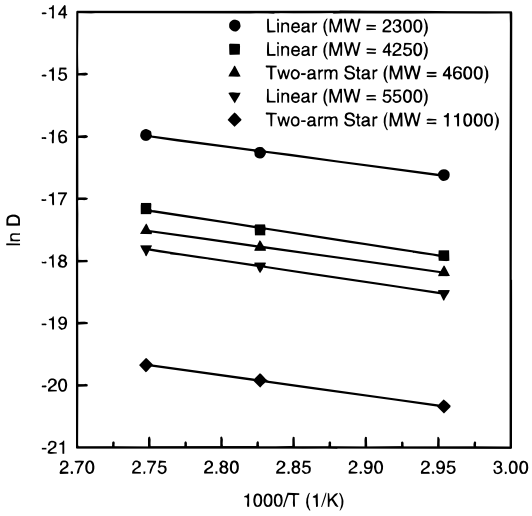

Figure 4. Self-diffusion coefficients of linear and two-arm PEOs with arm molecular weights of 2300 and 5500. The self-diffusion coefficients of MPEO (MW = 4250) are also included.

vibrations of the single OH end group of the linear PEO. Note that the hydrogen bonding must be formed intermolecularly. However, the 3500 cm^{-1} band is not detected for the two-arm PEOs (Figure 3). The band at 1720 cm^{-1} corresponds to the ketone (C═O) stretching vibration resulting from the coupling agent located at the center of the PEO chains.

In order to investigate how the defects affect on the PEO crystal structure, WAXD patterns for the linear and two-arm PEOs with M_a = 2300 and 5500 were taken after samples were crystallized and annealed at 46 °C for a prolonged time and then cooled to room temperature. All of the PEO crystals show close diffraction peak positions with very minor shifts during the initial stage of crystallization (see below in Figure 6, for example). Therefore, the defect does not appear to affect the crystal structure of the PEOs.

The self-diffusion coefficients (D) were measured at three different temperatures using PGSE-NMR for both linear and two-arm PEOs and are shown in Figure 4. It can be observed that the self-diffusion coefficients of the linear PEOs are greater (faster) than those of the

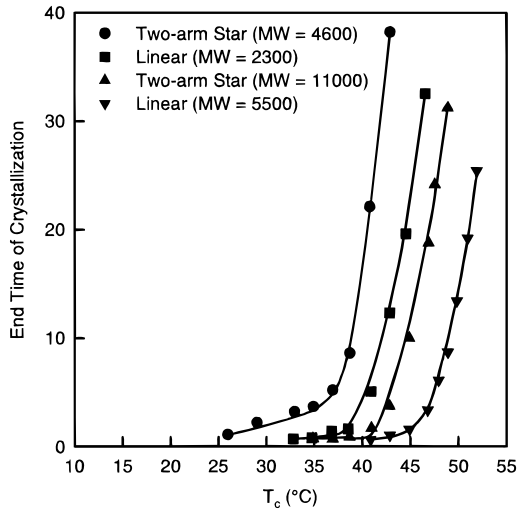

Figure 5. The change in the end time of isothermal crystallization with temperature for PEO (M_a = 2300 and 5500).

two-arm PEOs since the two-arm PEOs possess twice the molecular length of the linear ones. As shown in Figure 4, the self-diffusion coefficients of an α,ω-methoxypoly(ethylene oxide) (MPEO) with a MW = 4250 are greater than those of the two-arm PEO (M_a = 2300) at the same temperature although both fractions have a similar molecular length. This reflects the effect of the defects at the center of the two-arm PEO chains. The temperature dependence of D in Figure 4 can be described in terms of the Arrhenius equation of $D(T) = D_0 \exp\{-E_a/kT\}$, where E_a is the activation energy for diffusion, D_0 is assumed to be temperature independent, and k is the Boltzmann constant. The activation energies of the linear and two-arm PEOs can thus be calculated. An $E_a = 28 \pm 2$ kJ/mol for these fractions is in good agreement with the data reported in our earlier work.[30]

Overall Crystallization and Melting. Figure 5 shows the relationship of the end time of the overall exothermic processes obtained from isothermal DSC experiments with different crystallization temperatures for both the linear and two-arm fractions. At T_c (crystallization temperature) = 41 °C, the linear PEO (MW = 2300) takes 5 min to reach the end of the exothermic process (the overall crystallization is complete), while it takes 23 min for the two-arm PEO (M_a = 2300). Similar observations can be made for the linear PEO (MW = 5500) and the two-arm PEO (M_a = 5500).

Time-resolved WAXD experiments were performed to study the isothermal crystallization behavior of the linear and two-arm PEOs (see Figure 6). The crystallinity develops continuously during the progress of crystallization in these fractions. The final crystallinities of the two-arm PEOs are slightly lower (less than 5%) than the linear ones after normalization of the weight of the PEO component. As the crystallinity develops, the WAXD reflection peak positions do not show drastic changes but only slightly shift to wider angles, suggesting that the crystal perfection occurs while the PEO crystal structure is not affected.

Figure 7 shows the DSC melting traces for linear PEO (MW = 2300), two-arm PEO (M_a = 2300), and MPEO (MW = 4250) fractions crystallized at the same undercooling. For MPEO (MW = 4250), two melting peaks (low and high) are clearly observed over a wide temperature range and slightly increased with T_c.[34] The

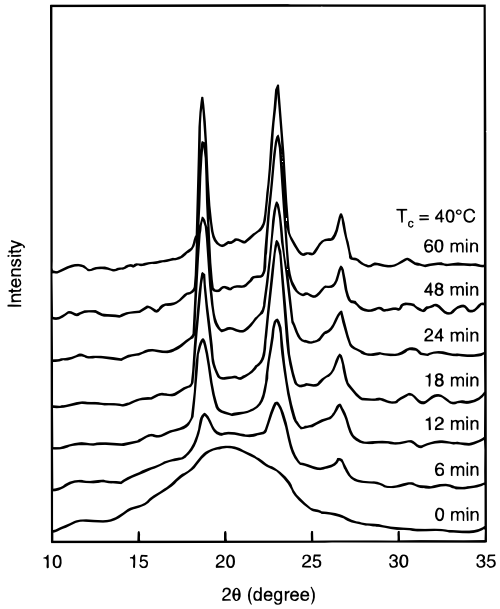

Figure 6. Time-resolved WAXD patterns for the two-arm PEO (M_a = 2300) crystallized at 40 °C from the melt.

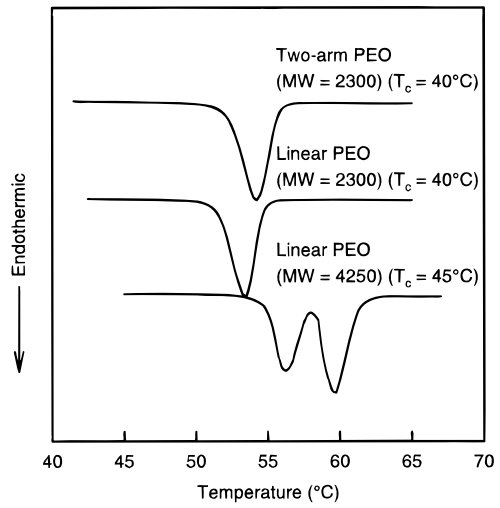

Figure 7. DSC melting curves for the linear PEO (MW = 2300), MPEO (MW = 4250), and two-arm PEO (M_a = 2300) fractions crystallized at roughly the same undercooling.[34]

low-melting peak reaches a limit around 57 °C, and the high peak around 61 °C. The high-melting temperature is attributed to the melting of the extended chain crystals, while the low-melting peak corresponds to the once-folded chain crystals.[34] On the other hand, both the linear PEO (MW = 2300) and two-arm PEO (M_a = 2300) show a single melting peak at approximately 55 °C. As a result, the lamellar crystal fold lengths of these two fractions must be very similar.

It is apparent that even though both the two-arm PEO and MPEO fractions have similar molecular weights and linear shapes, they show very different melting behavior. The melting peak temperature of the two-arm PEO (M_a = 2300) is close to the low-melting peak temperature of the MPEO (MW = 4250), which corresponds to the melting of once-folded chain crystals, but is 6 °C lower than the melting temperature of the extended chain crystals of MW = 4250. Therefore, the melting behavior of the two-arm PEO exclusively depends on the MW of each arm. We may attribute this difference in the melting behavior to the defects located at the center of the two-arm PEO molecules, and the

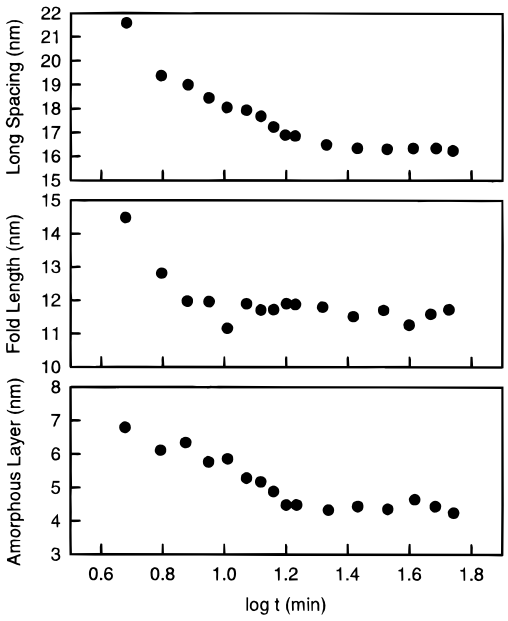

Figure 8. Long spacing, fold length, and amorphous layer thickness *versus* time for two-arm PEO (M_a = 2300) crystallized at 42 °C.

thickness of the lamellar crystal in this fraction is limited by the length of each arm.

The melting behaviors of the PEO fractions having MW = 5500 are more complicated than those having MW = 2300, since the former is not limited to forming extended chain crystals. However, a general similarity can still be found in the linear PEO (MW = 5500) and two-arm PEO (M_a = 5500).[35]

Nonintegral and Integral Folding Chain Crystal Formation. On the basis of overall crystallization and melting experiments, an important question arises. Does a two-arm PEO molecule behave as a whole chain, or does it recognize its defect during the initial stage of crystallization? Time-resolved SAXS experiments for both linear and two-arm PEOs at various crystallization temperatures may answer this question. In the SAXS data treatment, the correlation function method[33] was used to obtain long spacing, crystal fold length, and amorphous layer thickness. The changes of these parameters with isothermal crystallization time are shown in Figure 8 for the two-arm PEO (M_a = 2300) crystallized at T_c = 42 °C as an example.

In the initial stage of crystallization, a single scattering peak develops with a long spacing of 22.0 nm and a fold length of 15.0 nm. If one considers the fact that each arm of the PEO (M_a = 2300) has an extended length of 14.5 nm while the extended chain length of the two-arm PEO is 30.0 nm (the size of coupling agent is approximately 1.0 nm). It is evident that in the initial stage of crystallization the two-arm PEO molecule seems to behave as a whole chain length having a MW of about 4600. In fact, the initial long spacing of 22.0 nm is close to that of MPEO (MW = 4250) crystallized at the same undercooling.[34] Therefore, the two-arm PEO molecules more or less disregard the defect located at the center of the chain in the initial stage of crystallization. Thus, the initial conformation appears to preferentially form a fold length between once-folded and extended chain crystals of a hypothetical linear MPEO (MW = 4600). This implies that the two-arm PEO grows NIF crystals first in a transient state. As a result, the defect may be included in the crystal in this stage of crystallization.

An interesting aspect of the crystallization of the two-arm PEO is the subsequent thinning process. This differs from linear MPEO (MW = 4250), which exhibits both a thickening and a thinning processes.[34] As shown in Figure 8, although the long spacing, fold length, and amorphous layer all decrease over time, the decrease of the fold length occurs at a slightly faster rate than the other two parameters. After crystallization is complete for the two-arm PEO (M_a = 2300) (indicated by the end time in Figure 5), the long spacing plateaus at around 17.0 nm. On the basis of the size of the coupling agent (approximately 1.0 nm on each side), the true long spacing attributed to the PEO component should be around 15.0 nm. This corresponds well to the long spacing of the extended chain crystals formed in linear PEO (MW = 2300),[35] implying that the initial NIF crystals are transformed to lamellar crystals with a long spacing equivalent to the length of a single arm. The defects may thus migrate to both sides of the lamellar surface.

In the two-arm PEOs, both thickening and thinning should be possible for an individual molecule. However, the SAXS intensity is enhanced by the electron density (ED) difference in the samples. In the initial stage of crystallization, SAXS observations are attributed to the ED difference between the NIF crystalline and amorphous region in which the defects are more or less randomly distributed. Regardless of whether thickening or thinning of a single molecule occurs, the resulting SAXS changes will always exhibit a decrease in the long spacing due to an accumulation of defects on both sides of the lamellar surfaces, creating a periodic change of the ED. Thus, two molecular conformations are possible in the crystals. Each arm of a two-arm PEO molecule may be incorporated in neighboring lamellae, corresponding to molecular thickening (extended conformation), or may be located in the same lamellar crystal, corresponding to molecular thinning (once-folded conformation). Note that both the molecular processes require chain diffusion along the crystallographic *c*-axis. On the basis of our previous study, this type of molecular sliding motion along the chain direction in PEO crystals can occur even when the end groups are as big as the phenoxy groups.[9] Further research is necessary to study the conformational changes during the NIF → IF transformation.

With decreasing crystallization temperature, the initial long spacing and fold length of the NIF crystal decrease, as shown in Figure 9. Although both exhibit different slopes and intercepts, the linear relationship between the fold length of the NIF crystals and reciprocal undercooling qualitatively agrees with the nucleation theory, which predicts the relation $l \propto 1/\Delta T$.[36−45]

Similar but more complicated results can be observed in the two-arm PEO (M_a = 5500). For example, after crystallization at 43 °C for a prolonged time period, the initial long spacing of 22.7 nm gradually decreases to 19.5 nm, which is about 2.0 nm thicker than the long spacing of once-folded chain crystals of MW = 5500 (17.5 nm). Since the longer arm length leads to a lower density of defects (coupling agents), the effect of the defects on crystallization decreases. In addition, the molecular thickening and/or thinning processes in the two-arm PEOs having a longer arm length are also hampered.

Linear Crystal Growth Rates. Linear crystal growth rates were measured for the linear and two-arm PEOs based on the growth of spherulites at T_c < 35 °C

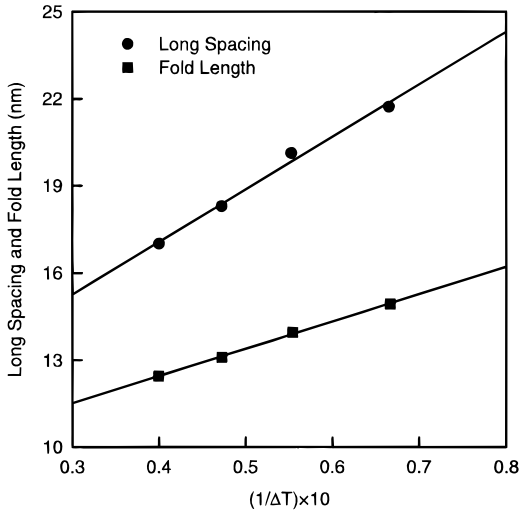

Figure 9. Relationships between the long spacing and fold length of two-arm PEO (M_a = 2300) and the reciprocal undercooling.

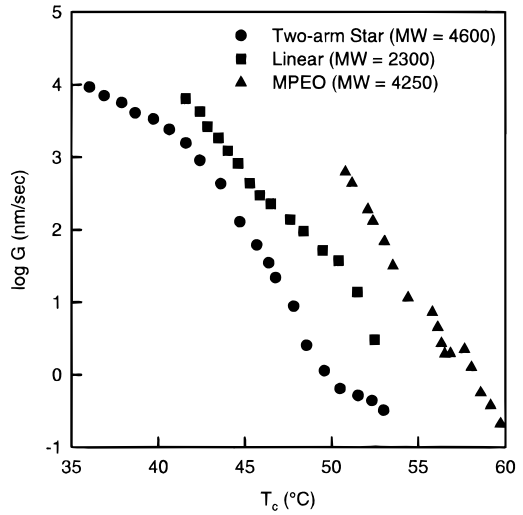

Figure 10. Linear crystal growth rates of the linear PEO (MW = 2300), MPEO (MW = 4250), and the two-arm PEO (M_a = 2300) fractions.

and single crystals at T_c > 35 °C. Figure 10 shows the relationship between the logarithmic growth rate and temperature for the PEOs. It is evident that all of the PEOs exhibit independent hyperbolic branches. The growth rates of the two-arm PEO (M_a = 2300) are generally slower than those of the linear PEO (MW = 2300) at a given undercooling. In this figure, the linear growth rate of MPEO (MW = 4250) is also provided for comparison.[34] The difference between the crystal growth rates of the linear PEO (MW = 5500) and the two-arm PEO (M_a = 5500) is smaller than that observed between the linear and two-arm PEOs with the shorter arm length.

The fact that the growth rates for two-arm PEOs are slower than those of linear PEOs at the same undercooling can be explained by considering the geometrical hindrance of the defects on the crystal growth surface. When a two-arm molecule is absorbed onto the growth surface, the coupling agent may be located on the surface, forming defects due to their large volume and noncrystallographic geometry.[46,47] These defects increase the surface free energy and, thus, the nucleation barrier, in turn leading to the decrease in the crystal growth rates. Only in the final IF crystals do the defects aggregate on the surfaces of the lamellar crystals. Furthermore, the juxtaposition of the growth branches corresponds to the changes in the crystal morphology (faceting−rounding−refaceting, see below).

Single Lamellar Crystal Morphologies. It is commonly known that changes in the linear growth rates with temperature are closely associated with crystal morphological changes. Thus, morphological observations can provide insight into the effect which defects have on the shape of single lamellar crystals. The morphological changes in single lamellar crystals of linear PEO (MW = 2300) are very similar to those reported previously.[5,13−17] In brief, at a T_c = 34 °C, only spherulites with irregular Maltese crosses are found. When the crystallization temperature is increased to 41 °C, single lamellar crystals with rounded shape are observed. When the temperature is increased to 44 °C, the crystal shape undergoes a major change, becoming hexagonal (faceting process), having two (100) planes along the *W* direction and four (140) planes along the *H* direction (see Figure 11 for definition). This morphology is retained at T_c = 46 °C. Above this temperature, all faces and apexes of the hexagonal crystals gradually become rounded again and this rounded shape remains up to T_c = 48 °C (rounding process). The rounded faces are again tangential to the (140) planes along the *H* direction with a slight truncation normal to the 010 direction. Further increase of the temperature above 50 °C leads to a hexagonal shape again (refaceting process). The temperatures where faceting−rounding−refaceting occur correspond to the undercoolings where the changes in the growth rates are observed.

Figure 11a−f shows single crystals grown at different crystallization temperatures for the two-arm PEO (M_a = 2300). The morphologies observed in the high undercooling range are similar to those observed for the linear PEO. The only difference is that the rounded morphology (Figure 11b−d) changes to a faceted one at T_c = 52 °C (Figures 11f) in which the single crystal observed exhibits a rectangular shape having two (100) and two (010) planes rather than a hexagonal one. The rectangular-shaped single crystal may originate from the defect packing on the surface of the lamellar crystals. Figure 12 shows one possible way that the two-arm PEO chains may be arranged differently from the linear PEO. For the linear PEO, the folding direction is expected to be parallel to the (120) planes.[15,48] In the case of the two-arm PEOs crystallized at very low undercoolings, the molecules adjust themselves on the crystal growth front to form IF crystals. This implies that, in an isolated single lamellar crystal, the coupling agent of the two-arm PEO molecules may directly become a part of folds on the lamellar surfaces and each arm possesses an extended chain conformation. The coupling agents possess a length of approximately 1.0 nm, while the distance of adjacent folding sites along the (120) planes is about 0.46 nm. As a result, it may be difficult to fold along the (120) planes since the energy penalty to fold in this manner is high. A folding direction along the (010) planes (the distance of 0.65 nm) or the (100) planes (the distance of 0.66 nm) is perhaps more realistic than along the (120) planes (Figure 12). However, the folding may also change entirely during this process. Electron diffraction and fold surface analysis are necessary to verify this explanation.

The linear PEO (MW = 5500) also exhibits single crystal morphology similar to that observed by Kovacs *et al.* for a similar MW fraction.[13] With increasing

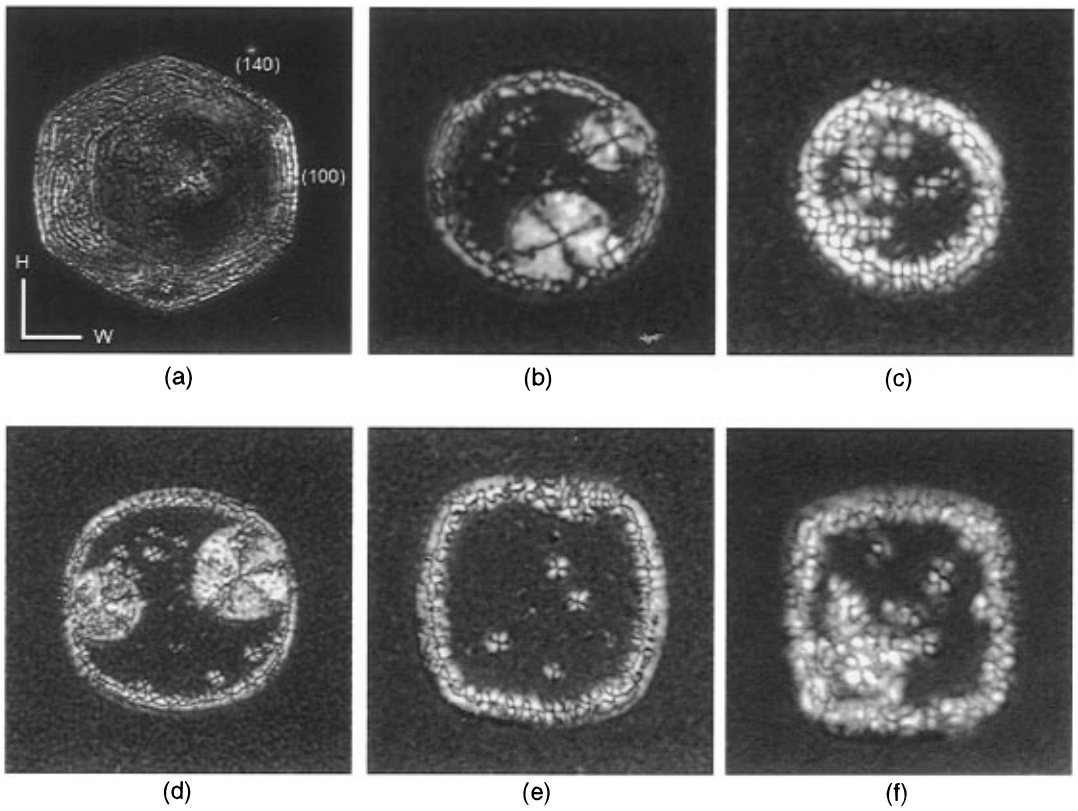

Figure 11. Single crystal morphologies for two-arm PEO (M_a = 2300) at different temperatures: (a) 44 °C, (b) 46 °C, (c) 47 °C, (d) 49 °C, (e) 50 °C, and (f) 52 °C.

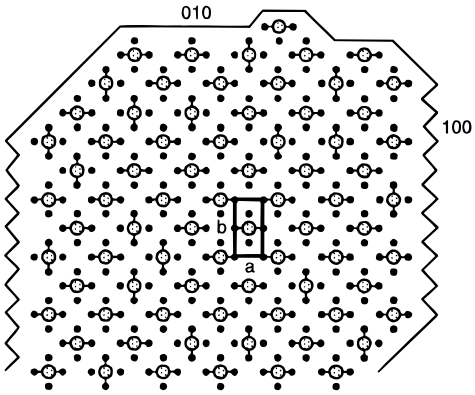

Figure 12. The crystal packing model for two-arm PEO. The folding direction is along the (010) planes as an example. The large, shadowed circles represent defects (coupling agents) and the line connections are schematic representatives of the folds. The small solid circles are crystal lattice points.

temperature, a faceting−rounding−refaceting phenomenon can be found. For the two-arm PEO (M_a = 5500), the single crystal morphology is similar to that of linear PEO (MW = 5500) for T_c < 53 °C. In the temperature range of 53−55 °C, the difference between the linear and the two-arm PEOs is not as obvious as that of the PEOs with a shorter chain length of M_a = 2300. Note that for the two-arm PEO (M_a = 2300), each arm can only assume an extended conformation in the crystals. For the PEO (M_a = 5500), each arm may either be extended or once-folded. The overall maximum number of folds for the entire molecule is thus three (triply-folded). The crystal growth rate in this temperature region is relatively fast, and NIF crystals form during the initial crystallization. The folding direction of each arm may, therefore, occur along the (120) planes similar to the crystals of linear PEO (MW = 5500). However, at T_c = 60 °C rectangularly shaped single crystals of two-arm PEO (M_a = 5500) begin to appear since each arm with M_a = 5500 now possesses an extended conformation. This is thus the same observation as in the case of two-arm PEO (M_a = 2300) at T_c = 52 °C.

Conclusion

Well-defined low MW two-arm PEO fractions with a defect at the center of each molecule have been designed to study the effect of the chain defect on crystallization, melting, and crystal morphology. An interesting result is that, in the initial stage of crystallization, the two-arm PEO molecules may act as a whole chain length to form the NIF crystals, disregarding the defect existing at the center of the chains. These defects are recognized at a later stage of the crystallization process, and gradually migrate to both sides of the lamellar surfaces *via* an apparent thinning process to form the IF crystals. As a result, the final fold length of the IF crystals in the two-arm PEO fractions are closely associated with the length of each arm rather the length of the entire molecule. The crystallization kinetics, including both the overall crystallization rate and the linear growth rate of the two-arm PEOs, is slower than those of linear PEOs having molecular lengths corresponding to both the individual arm as well as the whole molecule. This indicates that the existence of the defects hampers the crystal growth. The rectangularly shaped single lamellar crystals of the two-arm PEO fractions grown at low undercoolings exhibit (100) and (010) plane faceting, possibly due to a change in the folding direction caused by the large coupling agent size.

Acknowledgment. This work was supported by the Division of Materials Research, the National Science Foundation.

References and Notes

(1) Ungar, G.; Keller, A. *Polymer* **1986**, *27*, 1835.
(2) Ungar, G.; Keller, A. *Polymer* **1987**, *28*, 1899.
(3) Cheng, S. Z. D.; Zhang, A.-Q.; Chen, J.-H.; Heberer, D. P. *J. Polym. Sci. Polym. Phys. Ed.* **1991**, *29*, 287.
(4) Cheng, S. Z. D.; Chen, J.-H.; Zhang, A.-Q.; Heberer, D. P. *J. Polym. Sci. Polym. Phys. Ed.* **1991**, *29*, 299.
(5) Cheng, S. Z. D.; Chen, J.-H. *J. Polym. Sci. Polym. Phys. Ed.* **1991**, *29*, 311.
(6) Cheng, S. Z. D.; Zhang, A.-Q.; Barley, J. S.; Chen, J.-H.; Habenschuss, A.; Zschack, P. R. *Macromolecules* **1991**, *24*, 3937.
(7) Cheng, S. Z. D.; Chen, J.-H; Zhang, A.-Q.; Barley, J. S.; Habenschuss, A.; Zschack, P. R. *Polymer* **1992**, *33*, 1140.
(8) Cheng, S. Z. D.; Chen, J.-H.; Barley, J. S.; Zhang, A.-Q.; Habenschuss, A.; Zschack, P. R. *Macromolecules* **1992**, *25*, 1453.
(9) Cheng, S. Z. D.; Wu, S. S.; Chen, J.-H.; Zhuo, Q.; Quirk, R. P.; von Meerwall, E. D.; Hsiao, B. S.; Habenschuss, A.; Zschack, P. R. *Macromolecules* **1993**, *26*, 5105.
(10) Arlie, J. P.; Spegt, P. A.; Skoulios, A. E. *Makromol. Chem.* **1966**, *99*, 170.
(11) Arlie, J. P.; Spegt, P. A.; Skoulios, A. E. *Makromol. Chem.* **1967**, *104*, 212.
(12) Spegt, P. *Makromol. Chem.* **1970**, *139*, 139.
(13) Kovacs, A. J.; Gonthier, A. *Colloid Polym. Sci.* **1972**, *250*, 530.
(14) Kovacs, A. J.; Gonthier, A.; Straupe, C. *J. Polym. Sci. Polym. Symp.* **1975**, *50*, 283.
(15) Kovacs, A. J.; Straupe, C.; Gonthier, A. *J. Polym. Sci. Polym. Symp.* **1977**, *59*, 31.
(16) Kovacs, A. J.; Straupe, C. *J. Crystal Growth* **1980**, *48*, 210.
(17) Kovacs, A. J.; Straupe, C. *Faraday Discuss. Chem. Soc.* **1979**, *68*, 225.
(18) Hartly, A.; Leung, Y. K.; Booth, C.; Shepherd, I. W. *Polymer* **1976**, *17*, 354.
(19) Fraser, M. J.; Marshall, A.; Booth, C. *Polymer* **1977**, *18*, 93.
(20) Ashman, P. C.; Booth, C. *Polymer* **1973**, *14*, 300.
(21) Cooper, D. R.; Booth, C. *Polymer* **1977**, *18*, 164.
(22) Shimada, T,; Okui, N.; Kawai, T. *Makromol. Chem.* **1980**, *181*, 2643.
(23) Galin, J.-C.; Spegt, P.; Suzuki, S.; Skoulios, A. E.*Makromol. Chem.* **1974**, *175*, 991
(24) Thierry, A.; Skoulios, A. E. *Colloid Polym. Sci.* **1977**, *255*, 334.
(25) Thierry, A.; Skoulios, A. E. *Eup. Polym. J.* **1977**, *13*, 169.
(26) Wunderlich, B.; Melillo, L. *Makromol. Chim.* **1968**, *118*, 250.
(27) Hikosaka, M.; Tsukijima, K.; Rastogi, S.; Keller, A. *Polymer* **1992**, *33*, 2502.
(28) Hikosaka, M.; Rastogi, S. Keller, A.; Kawabata, H. *J. Macromol. Sci. Phys.* **1992**, *B31* (1), 87.
(29) von Meerwall, E. D. *Adv. Polym. Sci.* **1983**, *54*, 1; see also, *Rubber Chem. Technol.* **1985**, *58*, 527.
(30) Cheng, S. Z. D.; Barley, J. S.; von Meerwall, E. D. *J. Polym. Sci. Polym. Phys. Ed.* **1991**, *29*, 515.
(31) von Meerwall, E. D.; Palunas, P. *J. Polym. Sci. Polym. Phys. Ed.* **1987**, *25*, 1439.
(32) Ferry, J. D. *Viscoelastic Properties of Polymers*, 3rd ed.; Wiley: New York, 1980; p 136.
(33) Strobl, G. R.; Schneider, M. *J. Polym. Sci. Polym. Phys. Ed.* **1980**, *18*, 1343.
(34) Chen, J.-H. Ph.D dissertation, The Department of Polymer Science, The University of Akron, Akron, Ohio 44325-3909, 1992.
(35) Lee, S.-W. Ph.D dissertation, The Department of Polymer Science, The University of Akron, Akron, Ohio 44325-3909, 1994.
(36) Lauritzen, J. I. Jr.; Hoffman, J. D. *J. Appl. Phys.* **1973**, *44*, 4340.
(37) Hoffman, J. D.; Frolen, L. J.; Ross, G. S.; Lauritzen, J. I., Jr. *J. Res. Natl. Bur. Stand. Sect. A* **1975**, *79A*, 671.
(38) Hoffman, J. D.; Davis, G. T.; Lauritzen, J. I., Jr. In *Treatise on Solid State Chemistry*; Hannay, N. B., Ed.; Plenum: New York, 1976; Vol. 3, Chapter 7, pp 497−614.
(39) Hoffman, J. D. *Polymer* **1982**, *23*, 656; **1983**, *24*, 3.
(40) Hoffman, J. D.; Miller, R. L. *Macromolecules* **1988**, *21*, 3038.
(41) Hoffman, J. D. *Macromolecules* **1986**, *19*, 1124.
(42) Buckley, C. P. *Polymer* **1980**, *19*, 444.
(43) Sadler, D. M. *J. Polym. Sci. Polym. Phys. Ed.* **1985**, *23*, 1533.
(44) Skoulios, A. E. *Kolloid Z. Z. Polym.* **1969**, *234*, 1059.
(45) Gilg, P. B.; Skoulios, A. E. *Makromol. Chem.* **1971**, *140*, 149.
(46) Sadler, D. M. Polymer **1983**, *24*, 1401; **1987**, *28*, 1440.
(47) Hoffman, J. D. *Polymer* **1985**, *26*, 1763.
(48) Chen, J.; Cheng, S. Z. D.; Wu, S. S.; Lotz, B.; Wittmann, J.-C. *J. Polym. Sci. Polym. Phys. Ed.* **1995**, *33*, 1851.

MA960048Q